

Northumbria Research Link

Citation: Yang, Tao, Chen, Wenge, Zhang, Hui and Fu, Yong Qing (2022) Interfacial bonding characteristics of in-situ synthesized graphene-coated copper nanocomposite powders using wheat flour precursor. *Journal of Materials Science*, 57 (41). pp. 19309-19326. ISSN 0022-2461

Published by: Springer

URL: <https://doi.org/10.1007/s10853-022-07821-5> <<https://doi.org/10.1007/s10853-022-07821-5>>

This version was downloaded from Northumbria Research Link:
<https://nrl.northumbria.ac.uk/id/eprint/50305/>

Northumbria University has developed Northumbria Research Link (NRL) to enable users to access the University's research output. Copyright © and moral rights for items on NRL are retained by the individual author(s) and/or other copyright owners. Single copies of full items can be reproduced, displayed or performed, and given to third parties in any format or medium for personal research or study, educational, or not-for-profit purposes without prior permission or charge, provided the authors, title and full bibliographic details are given, as well as a hyperlink and/or URL to the original metadata page. The content must not be changed in any way. Full items must not be sold commercially in any format or medium without formal permission of the copyright holder. The full policy is available online: <http://nrl.northumbria.ac.uk/policies.html>

This document may differ from the final, published version of the research and has been made available online in accordance with publisher policies. To read and/or cite from the published version of the research, please visit the publisher's website (a subscription may be required.)

Interfacial bonding characteristics of *in-situ* synthesized graphene-coated copper nanocomposite powders using wheat flour precursor

Tao Yang¹, Wenge Chen^{1,*}, Hui Zhang¹, Yong-Qing Fu^{2,*}

¹ School of Materials Science and Engineering, Xi'an University of Technology, Xi'an, Shaanxi, 710048, P.R. China.

² Faculty of Engineering and Environment, Northumbria University, Newcastle upon Tyne, NE1 8ST, UK.

Abstract: It is quite difficult to *in-situ* synthesize graphene directly and economically onto surfaces of copper powders as a reinforcement phase for metal matrix composites, and few studies have been focused on interfacial bonding characteristics between graphene (Gr) layer and copper powders. This paper explores a new strategy using wheat flour as a precursor to *in-situ* generate graphene on the surfaces of copper powders and investigates interfacial bonding characteristics between Gr and copper powders. Results reveal that the *in-situ* generation process of graphene on the surfaces of copper powders has two critical stages. The first one is the low-temperature stage (up to 400 °C), in which H₂ reduces the oxide layer (Cu₂O) into metallic Cu on the surfaces of the copper powders. The second one is the high-temperature stage (from 289 to 800 °C), in which the copper powders, with their good catalytic properties, cause the break-up of chemical bonds of the flour and expose the carbon atoms, and

* Corresponding authors: Prof. Wenge Chen; Prof. Richard Y.Q.Fu.
E-mail: wgchen001@263.net (W.G. Chen), richard.fu@northumbria.ac.uk (Richard Y.Q. Fu)

then high affinity of copper and carbon atoms causes recombination of carbon atoms and formation of graphene. Interfacial structures of the graphene-coated copper composite powder show semi-coherent features with a lattice matching of $\text{Gr}_{\{002\}}//\text{Cu}_{\{111\}}$. The interfaces between Cu and Gr have not shown any intermediate phases or porous structures. These composite powders produced using such a low-cost but highly efficient process can be effectively used as an excellent reinforcement for metal matrix composites.

Keywords: Graphene-coated copper; In-situ; Interface; Solid carbon source

1. Introduction

Graphene (Gr) has its great potential to be used in electronic devices [1], aerospace [2], and biomedicine [3] due to its extraordinary physical and mechanical properties. A variety of preparation methods for graphene have been developed, including mechanical exfoliation [4], chemical exfoliation [5], and *in-situ* growth using physical and chemical methods [6]. Among these, mechanical exfoliation method is time-consuming and cannot easily obtain large-scale graphene [4]. Chemical exfoliation method usually uses graphite as a raw material and strong acids have been used for oxidation stratification, followed by a high temperature reduction treatment to obtain reduced graphene oxide (rGO) [5]. However, rGO is simply a derivative of graphene, and compared with graphene, there are a large amount of defects in the rGO, which limit its wide-range applications. Graphene prepared using the *in-situ* growth methods can achieve a high quality, thus receiving extensive

attention recently [6], and there are reports to *in situ* prepare graphene on silicon or silicon carbide [7].

There are a lot of interests recently to search for high quality reinforcing phases in metal matrix composites, and many researchers are focusing on the *in-situ* growth of graphene on a metal substrate for these purposes [8-11]. An early study for *in-situ* generation of graphene on the surface of a metal substrate was reported by Somani et al [8]. They chose Ni as the substrate, and synthesized graphene through *in-situ* thermal decomposition of a carbon source of camphor. In 2009, Li et al. [12] synthesized uniform graphene on copper substrates, and proposed a self-limiting growth mechanism of graphene on copper substrates, which easily produced a few layer or even single-layer graphene. Due to the strong demand for graphene reinforced composites for industry applications, there is an urgent need to *in-situ* generate high quality Gr on the surfaces of metallic powders, such as copper.

The commonly used carbon sources for synthesis of graphene include gas sources (such as methane/CH₄) [12], liquid sources (such as hexane and liquid paraffin) [9, 13], and solid sources (such as polymethyl methacrylate/PMMA, sucrose and glucose) [10, 11, 14, 15]. When the gaseous carbon source such as CH₄ is used, its decomposition temperature is generally around 1000 °C [12]. Such a high temperature is very close to the melting point of Cu powder, and thus it is extremely difficult to form the graphene-coated copper composite powders [16]. Using the solid carbon source, the decrease of decomposition temperature has been reported, and thus the carbon layer could be easily and uniformly distributed on all the powder surfaces

[10].

However, solid carbon sources are not widely available and its process is costly [10, 11]. Therefore, it is necessary to develop a cheap but effective method to synthesize Gr on the surfaces of metallic powders. On another matter, the solid carbon sources generally contain a lot of heteroatoms (such as oxygen) [11]. Since the ratio of carbon to oxygen in glucose ($C_6H_{12}O_6$) is $\sim 1:1$, it is difficult to explain why the oxygen atoms produced during high temperature process do not oxidize the copper matrix, as reported in Ref. [17]. For graphene-coated copper composite powders, the interfacial structure can significantly affect the enhancement effect of reinforcing phases in a metal matrix [14, 18-20].

In this study, we proposed a new strategy using low cost and widely available wheat flour as the solid precursor of graphene to *in-situ* generate graphene on the surfaces of copper powders, and then explored its *in-situ* growth mechanisms and studied the interfacial microstructures. The flour-processed copper composite powders with different carbon source contents were obtained using a ball milling process, and graphene-coated copper composite powders were obtained using *in-situ* generation process. Microstructures of the composite powders were characterized to identify the interfacial bonding characteristics between Gr and Cu, from which *in-situ* generation mechanism of graphene was proposed. The Gr@Cu composite powders prepared can be applied as a reinforcing components for metal matrix composites, which can be used in electric slide rail material, high voltage electrical contact material and electronic packaging materials, etc. [21-24].

2. Experimental materials and methods

2.1 Materials

Copper powders (purity 99.9%, 35-38 μm) were purchased from Beijing Xingrongyuan Technology Co., Ltd., China. The flour powders (universal wheat flour) were obtained from Chinese Resources Vanjia Convenient Supermarket. The rest of the reagents in this study (including anhydrous ethanol and nitric acid) were of analytical grade and used directly without further purification.

2.2 Preparation of flour@Cu composite powders

Fig. 1(a) schematically illustrates the synthesis process for the flour@Cu composite powder. Planetary ball milling (XQM-0.4L, China) was used to prepare flour@Cu composite powder. Firstly, 1.0 g of flour, 10 g of Cu powder and 110 g of stainless steel balls (with a diameter of 3 mm and a ball-to-material ratio of 10:1) were weighed and poured into a planetary ball milling tank. The flour-coated copper powder was obtained using the ball milling process at 423 rpm for 5 h, and this sample was named as 1.0flour@Cu. Afterwards, flour powders with different weights of 0.8 g, 0.5 g and 0 g were mixed with 10 g of copper powder using the above ball milling process (with a ball-to-material ratio 10:1), and they were named as 0.8flour@Cu, 0.5flour@Cu and flake Cu powders, respectively.

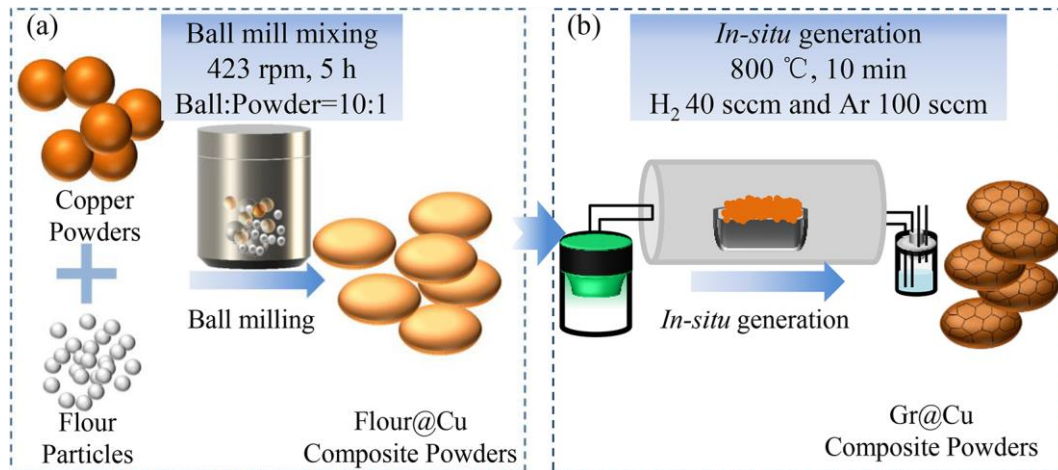


Fig. 1 Schematic illustrations of the preparation processes of composite powders. (a) flour@Cu composite powders, (b) Gr@Cu composite powders

2.3 Preparation of Gr@Cu composite powders

The flour@Cu composite powder was put into a corundum ark, before put into a vacuum tube furnace. The furnace was heated up to 800 °C with an increased rate of 10 min/°C, and calcined for 10 min. During this process, a gas mixture of 40 sccm H₂ and 100 sccm Ar was kept flowing into the chamber throughout to generate reduction and formation of Gr@Cu composite powder. The preparation process is illustrated in Fig. 1(b). We named the composite powders obtained after the *in-situ* reaction processes as 1.0Gr@Cu, 0.8Gr@Cu and 0.5Gr@Cu, respectively.

2.4 Testing and characterization methods

X-ray diffractometer (XRD, XRD-7000S, Japan, Cu K α radiation of 1.5418 Å, with a scanning speed of 8 °/min) was used to analyze the crystalline phases of the copper powder and composite powders. Scanning electron microscope (SEM, Quanta-450-FEG, USA, USA) was used to observe the morphology of the powder with an operating voltage of 20 kV, and the attached energy dispersive X-ray

spectroscopy (EDS) was used to assess if Gr was coated on the copper powders.

The copper particles of the Gr@Cu composite powder were etched away using a 20 wt.% nitric acid solution. The obtained product of Gr was washed several times with deionized water and ethanol. Raman spectroscopy (Renishaw inVia Raman Microscope, UK) analysis of samples was performed with 532 nm Ar⁺ laser to investigate the degree of Gr defects in the etched Gr@Cu samples. Microstructures and bonding interfaces of Gr and copper particles were characterized using a high-resolution transmission electron microscope (HR-TEM, TF200X, USA), and the lattice fringes and interfacial bonding characteristics of graphene and copper particles were characterized. Valence states and bond structures of 0.5Gr and 0.5Gr@Cu powders were analyzed using an X-ray photoelectron spectroscope (XPS, AXIS ULTRA, UK, Al K α X-ray ray source with an energy of 1486.6 eV). The base vacuum of the XPS chamber was 9.8×10^{-10} Torr, and the Casa XPS software was used to perform peak splitting and data Gaussian fitting processing.

3. Results and discussion

Figure 2 shows morphology and phase analysis results of the initial pure copper powder and the flake of copper powder after ball milling. The SEM image of pure copper powder in Fig. 2(a) shows that the copper powders are spherical with their sizes between 33 and 40 μm . In this study, we used the ball milling process of 423 rpm, a duration of 5 h, ball-to-material ratio (10:1) to change the original spherical copper powders into a flake of copper powders (Fig. 2(b)). It can be seen that the

spherical copper powder has been completely transformed into flake copper powder after ball milling, and the thickness of the flake layer is about 1~3 μm .

XRD pattern in Fig. 2(c) shows the (111) crystal plane of Cu_2O . The formation of oxides is because the copper powder is highly active and easily oxidized when it comes in contact with air.

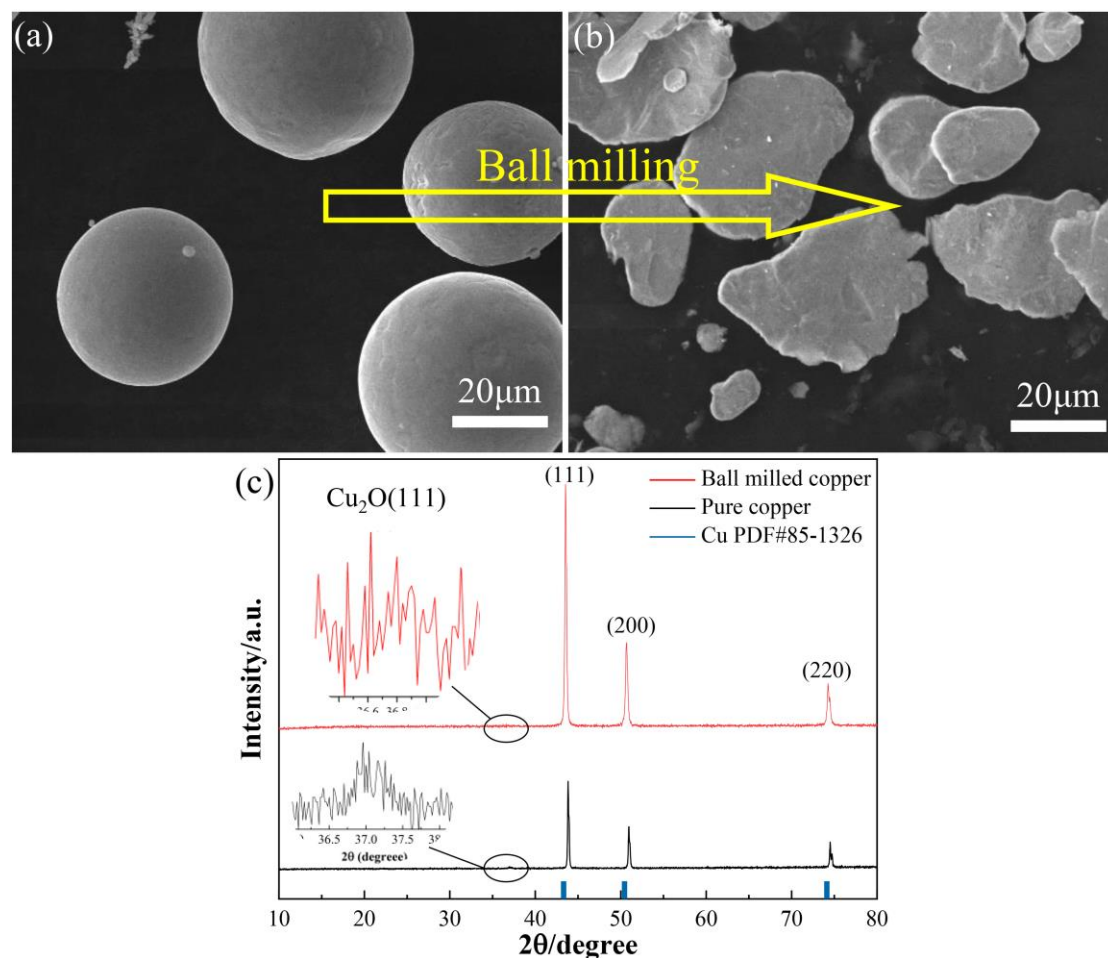


Fig. 2 SEM and XRD patterns of pure copper and ball-milled flake copper powder. (a) SEM image of pure Cu powder, (b) SEM image of flake Cu powder, (c) XRD pattern of pure Cu and flake Cu powder

After verifying that the ball milling can transform the spherical particles into flake particles, the same ball milling process was used to mix different contents of flour (1.0 g, 0.8 g, 0.5 g) with 10 g copper powder. Figs. 3(a) and 3(b) show the SEM

and EDS images of 1.0flour@Cu composite powder. The morphology of Cu powder in the composite powder is consistent with that in Fig. 2(b), and in both these two cases, they become flakes of powders. The surface of these flakes is coated with a thick substance, which becomes agglomerated as shown by the black arrow in Fig. 3(b). These substances are considered as the carbon source (e.g., a flour layer). EDS analysis of point A shows that it contains a large number of C and O atoms (the inset of Fig. 3(b)), clearly indicating that the agglomerates are associated with flour structures.

Figures 3(c), 3(d) and 3(e), 3(f) are SEM and EDS images of 0.8flour@Cu and 0.5flour@Cu composite powders, respectively. It can be seen that as the flour content is decreased, the agglomeration of the flour carbon source is gradually reduced. When the flour content is 0.5 g, no obvious agglomeration of flour is found in the SEM image (Fig. 3(f)), and the flour particles are firmly covered on the surfaces of the copper powders. The above phenomenon shows that a large carbon source content will cause agglomeration in the early mixing process, which may lead to the following phenomena. (1) The low solubility of carbon in copper substrates makes it unfeasible to produce multilayer graphene. In the process of *in-situ* graphene growth, due to the excessively large carbon source content in the agglomerated area, thicker layers of graphene-like nanoplatelets or graphite flakes will be produced if the catalytic limit of copper powder is exceeded. (2) The thicker carbon source is easily peeled off, and is scattered among the flakes of copper powders. It is easily carbonized into scattered graphite flakes during high-temperature carbonization. Based on the above results, it

is concluded that 0.5 g of flour is the best carbon source content for this study.

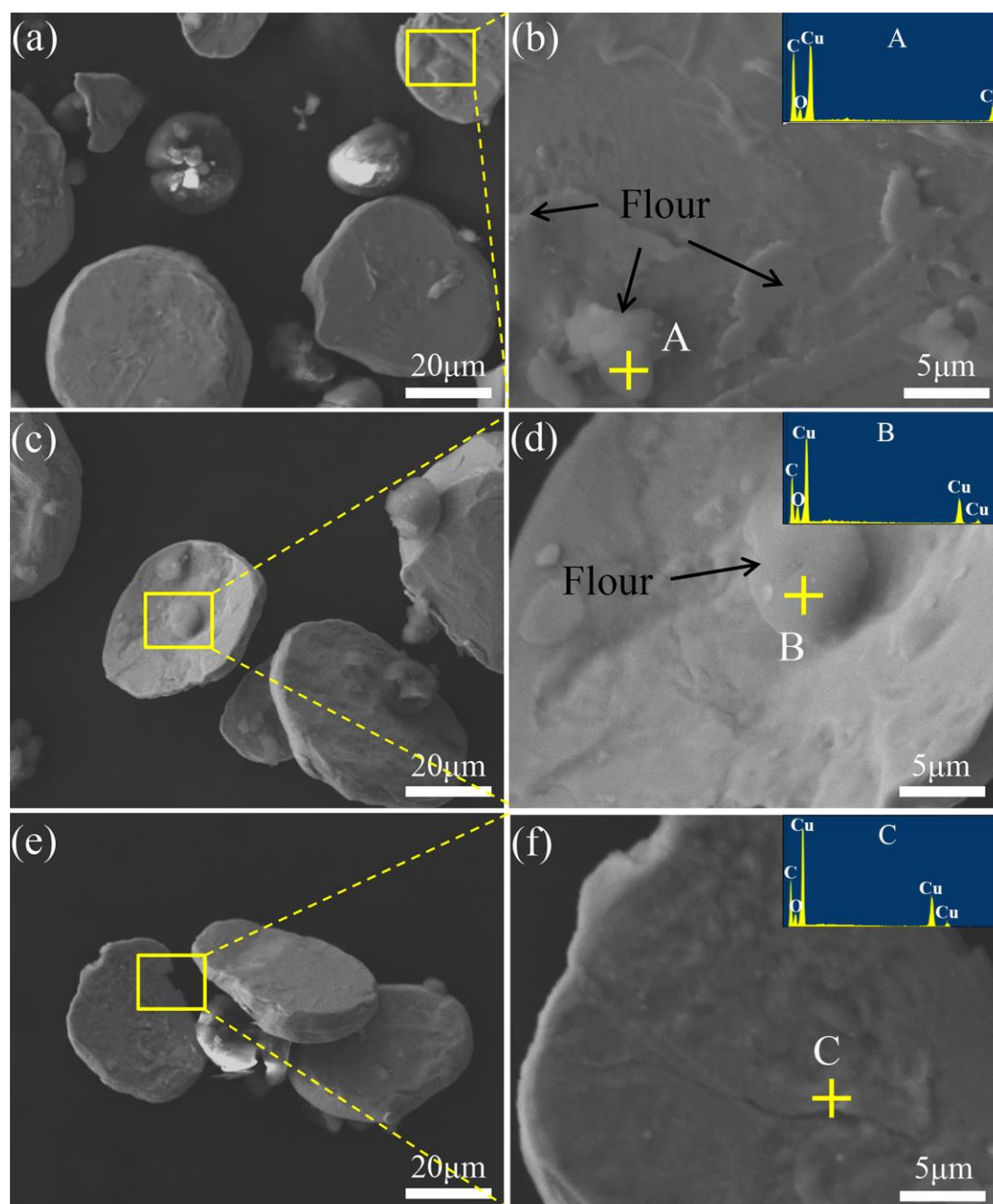


Fig. 3 SEM images and EDS results of different contents of flour@Cu composite powders. (a~b) SEM images of 1.0 flour@Cu composite powder, (c~d) SEM images of 0.8 flour@Cu composite powder, (e~f) SEM images of 0.5 flour@Cu composite powder. The illustrations are the EDS images at points A, B, and C respectively

For the Gr@Cu composite powders obtained after the *in-situ* generation, XRD

analysis was performed to investigate whether the oxide layer (e.g., Cu_2O as shown in Fig. 2(c)) on the surface of the original copper powder is still existed after the *in-situ* generation process of graphene. The whole processes have involved the following chemical reactions: (1) Cu_2O is oxidized to produce CuO . This is because the flour contains a large amount of oxygen elements. During heating, Cu_2O particles are preferentially oxidized by these oxygen elements to form CuO ; (2) Due to the presence of H_2 , the Cu_2O may undergo a reduction reaction during heating to generate metallic Cu particles.

It can be seen from Fig. 4 that the XRD patterns of three types of composite powders only show diffraction peaks at 43.03° , 50.2° , and 73.8° , corresponding to the (111), (200), and (220) planes of copper, respectively. The inset of Fig. 4 shows the diffraction peak regions of cuprous oxides, which clearly shows no diffraction peak. This reveals that the aforementioned Cu_2O (Fig. 2(c)) has been successfully reduced into Cu particles during the *in-situ* process. In addition, there is no diffraction peak of graphene in the XRD pattern. This may be due to the small amount of *in-situ* generated graphene, which is below the lower detection limit of XRD [25].

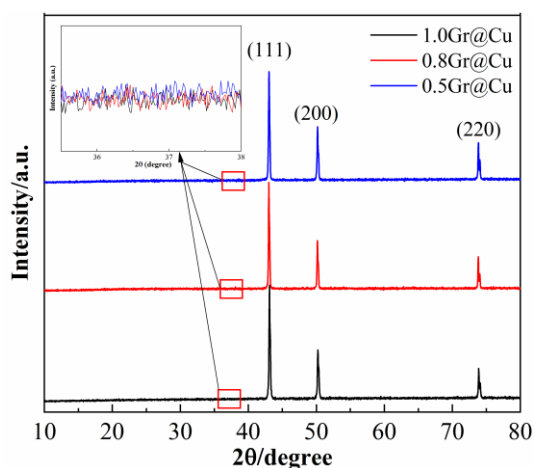


Fig. 4 XRD patterns of different Gr@Cu composite powders

Since the XRD pattern (Fig. 4) did not show the presence of graphene, SEM was then used to characterize the composite powder. Fig. 5 shows the SEM images of the Gr@Cu composite powder obtained by calcinating flour@Cu composite powder at 800 °C under the flowing of 40 sccm H₂ and 100 sccm Ar for 10 min. Figs. 5(a), 5(b) and Figs. 5(c), 5(d) are SEM images of 1.0Gr@Cu and 0.8Gr@Cu composite powders, respectively. It can be seen that a layer of carbon source is coated on the surface of the copper powder after high temperature reduction treatment, and this carbon source is successfully changed into graphene which shows a folded morphology (as indicated by the yellow arrow). The formation of graphene folds can be explained by the fact that the graphene has a negative thermal expansion coefficient ($-7 \times 10^{-6} \text{ K}^{-1}$) [26], and copper has a positive thermal expansion system ($16.6 \times 10^{-6} \text{ K}^{-1}$) [27]. During the cooling process, due to the mismatch of expansion coefficients of these two materials, the interfaces between graphene and copper are subjected to large thermal stress. Graphene is subjected to compressive stress and copper is subjected to tensile stress, which causes the significant folding of graphene [28].

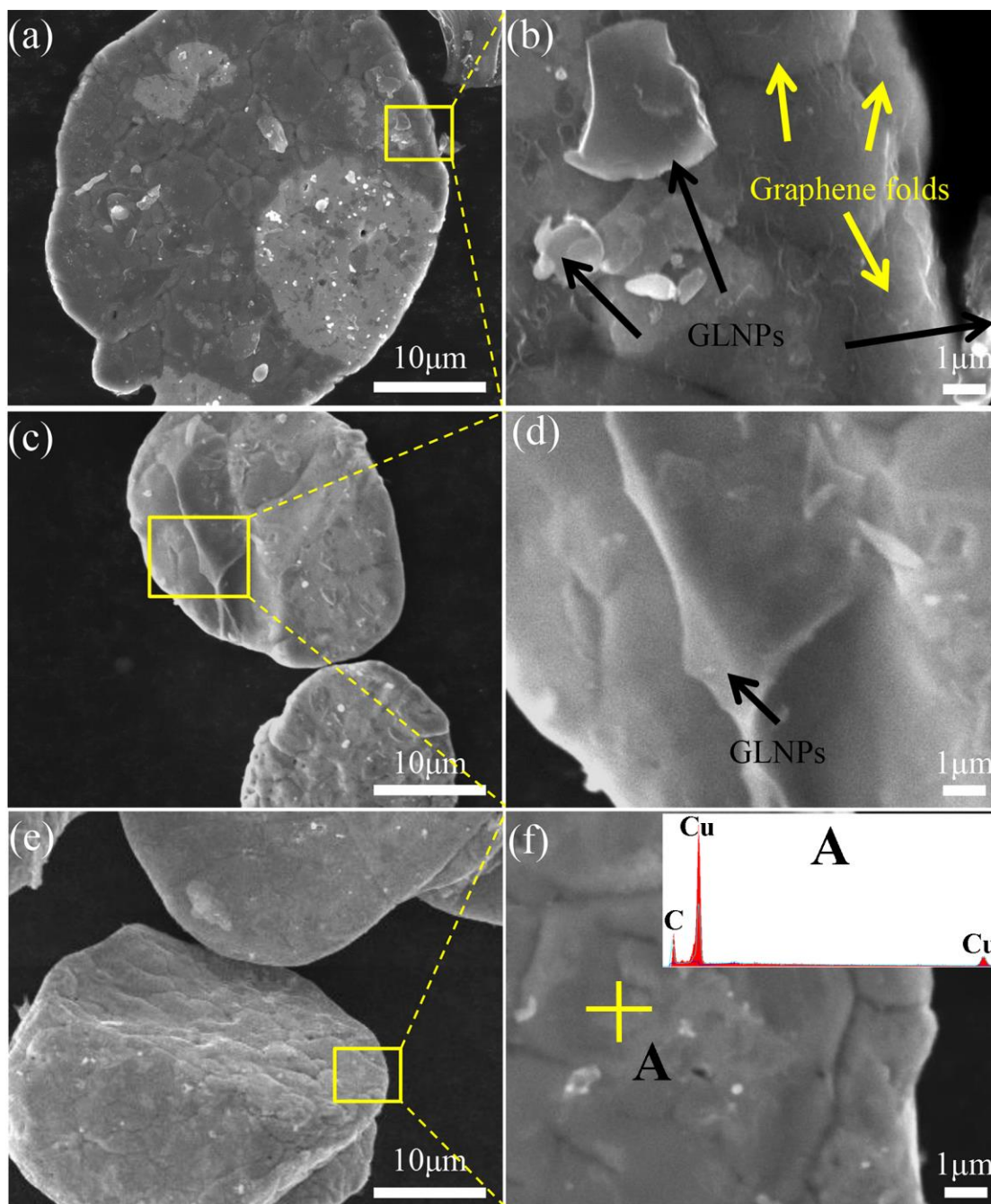


Fig. 5 SEM images of different Gr@Cu composite powders. (a~b) 1.0Gr@Cu composite powder, (c~d) 0.8Gr@Cu composite powder, (e~f) 0.5Gr@Cu composite powder. The illustration is the EDS image at point A

In addition, thick layers of bright and white substances (indicated by the black arrows) are observed in Figs. 5(b) and 5(d), and these are graphene-like nanoplatelets (GLNPs). These GLNPs are distributed on the surfaces of the copper powders and

scattered among the flake of copper powders. This confirms the previous observations based on the SEM images of 1.0flour@Cu and 0.8flour@Cu composite powders (Fig. 3(b), (d)), which show that flour agglomeration may cause undesirable consequences. The formation of GLNPs is mainly due to the large carbon content when using 1.0 g flour. After the first layer of graphene is formed on the surface of the copper powder, the excess carbon source can be continuously graphitized and grown on this layer, thus resulting in a much thicker layer of GLNPs [15, 18]. It is worthwhile to note that in the SEM images of the 0.5Gr@Cu composite powder (Figs. 5(e) and 5(f)), no GLNPs can be observed. Only a thin graphene layer can be observed on the surface of the copper powder, without obvious graphene folds. Previously Lee [18] et al. also reported that a few-layer graphene was *in-situ* generated on the surface of the nano-copper powder. Their SEM images of the graphene are consistent with the results in this paper, and their observed graphene did not show apparent folds. Therefore, we believe that 0.5 g of flour is the best carbon source content for the process parameters used in this study.

Raman spectra are often used to characterize the structural integrity of graphene. Raman spectra of graphene have three characteristic peaks, e.g., D peak, G peak and 2D peak. The D peak represents the defect peak of graphene, the G peak is produced by the stretching of sp^2 carbon-carbon bonds (C=C), and the 2D peak is generally related to the number of graphene layers [29]. The intensity ratio of the D peak to the G peak (I_D/I_G) is generally used to define the defect degree of graphene. The larger the I_D/I_G ratio is, the higher the defect degree of graphene is [30]. To verify the quality of

the graphene *in-situ* generated on the surface of the flake copper powders, Raman spectra analysis was carried out. Before the test, the Gr@Cu composite powder was etched in a 20 wt.% nitric acid solution to remove copper, thus eliminating the influence of the copper particles on the characteristic peaks of carbon. As shown in Fig. 6, the I_D/I_G ratio the characteristic D peak and G peak of graphene for all three Gr@Cu composite powders have their values between 0.89 and 0.91, which is less than the reported value of I_D/I_G of rGO (1.00~1.38) [31-34].

In order to verify the effect of short-term acid etching on the changes of degree of graphene defects, the Raman spectra of Gr@Cu before and after acid etching were tested (Supplementary Material Fig. S1 and Fig. 6). After comparison, it was proved that the ratio of I_D/I_G of the composite powder before and after etching does not change significantly, which indicates that short-term acid etching would not increase the defect states of graphene.

The D peak positions of 1.0Gr@Cu, 0.8Gr@Cu and 0.5 Gr@Cu composite powders are at 1334 cm^{-1} , 1338 cm^{-1} and 1340 cm^{-1} , respectively. The G peak positions are at 1588 cm^{-1} , 1591 cm^{-1} and 1592 cm^{-1} , respectively. With the decrease of carbon source content, the positions of D peak and G peak show clear blue shifts (e.g., the peaks are shifted to the higher band side). This is related to the increase in the compressive strain of Gr [32, 35].

Interestingly, the 2D regions show abnormal shapes in the Raman spectra from $2000\text{ to }3400\text{ cm}^{-1}$. This can be explained by the combined effect of the planar and non-planar structures of graphene [18]. In order to explain the broadening of the 2D

peaks, the Lorentz curve is used to deconvolute and fit the 2D region, and the deconvoluted results are shown in the inset of Figs. 6(a) to 6(c). The 2D area can be divided into 2D peaks, D+G peaks and 2D' peaks after fitting, and the D+G peak and 2D' peak are generated due to the strain in graphene with a non-planar structure [18, 36].

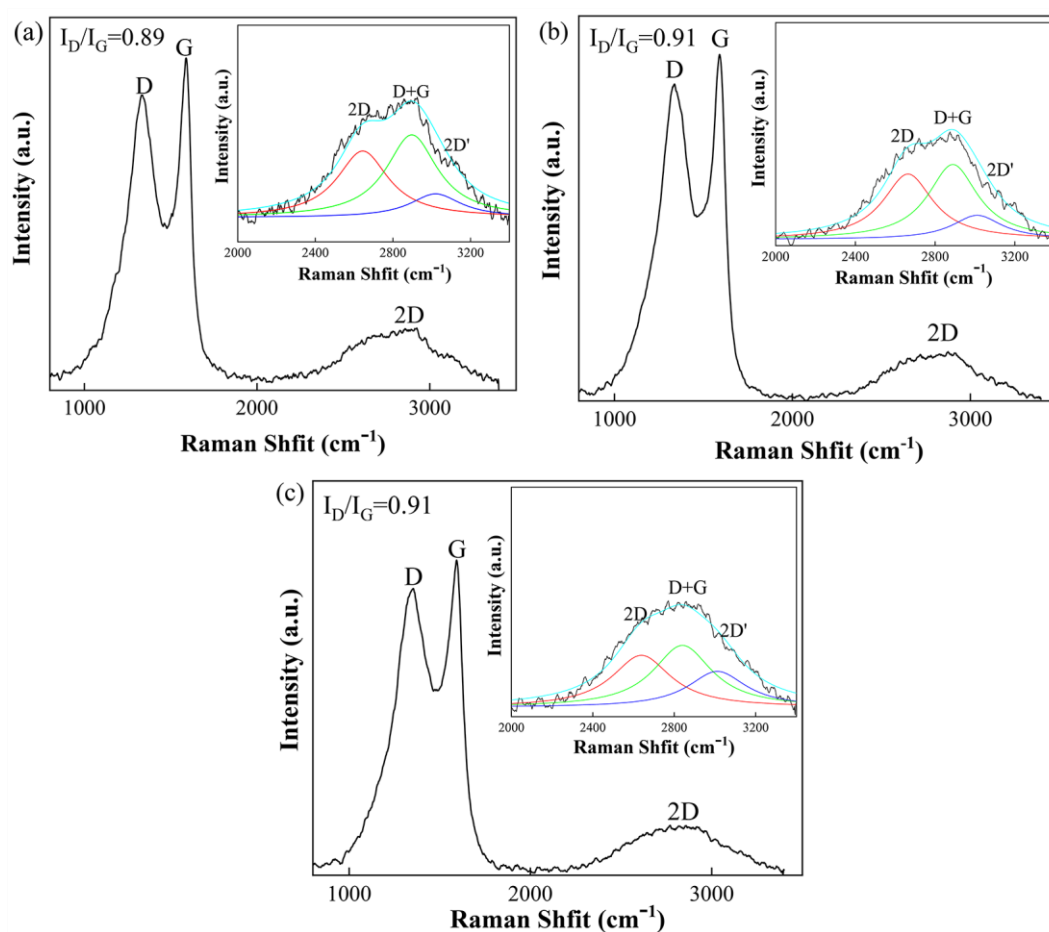


Fig. 6 Raman spectra of different Gr@Cu composite powders after acid etching. (a) 1.0Gr@Cu composite powder, (b) 0.8Gr@Cu composite powder, (c) 0.5Gr@Cu composite powder. The inset shows the 2D area fitted using the Lorentz curve

In order to characterize the quality of microstructure and interfacial structures of *in-situ* generated graphene, TEM was used to characterize the morphology of graphene and the interfacial bonding between graphene and copper powder. In

literature [24, 37], acid etching was used to remove part of the copper substrate, to observe the morphology and interface bonding state of graphene. In this paper, the same method was applied. Fig. 7 shows the TEM, HRTEM and EDS-mapping images of 0.5Gr@Cu composite powder after etching. It can be seen that the morphological features of the etched structures generally show gray color, and have obvious tulle-like graphene morphologies (Fig. 7(a)). In addition, there are small amounts of black particles (Fig. 7(c)). Based on the HRTEM image shown in Fig. 7(b), the gray area has a crystal interplanar distance same with that of Gr₍₀₀₂₎, indicating that the gray tulle-like substance is the *in-situ* generated graphene. The black particles can be confirmed as the copper particles from the EDS-mapping images (Figs. 7(e~g)). Interestingly, the O element does not appear in Figs. 7(e~g).

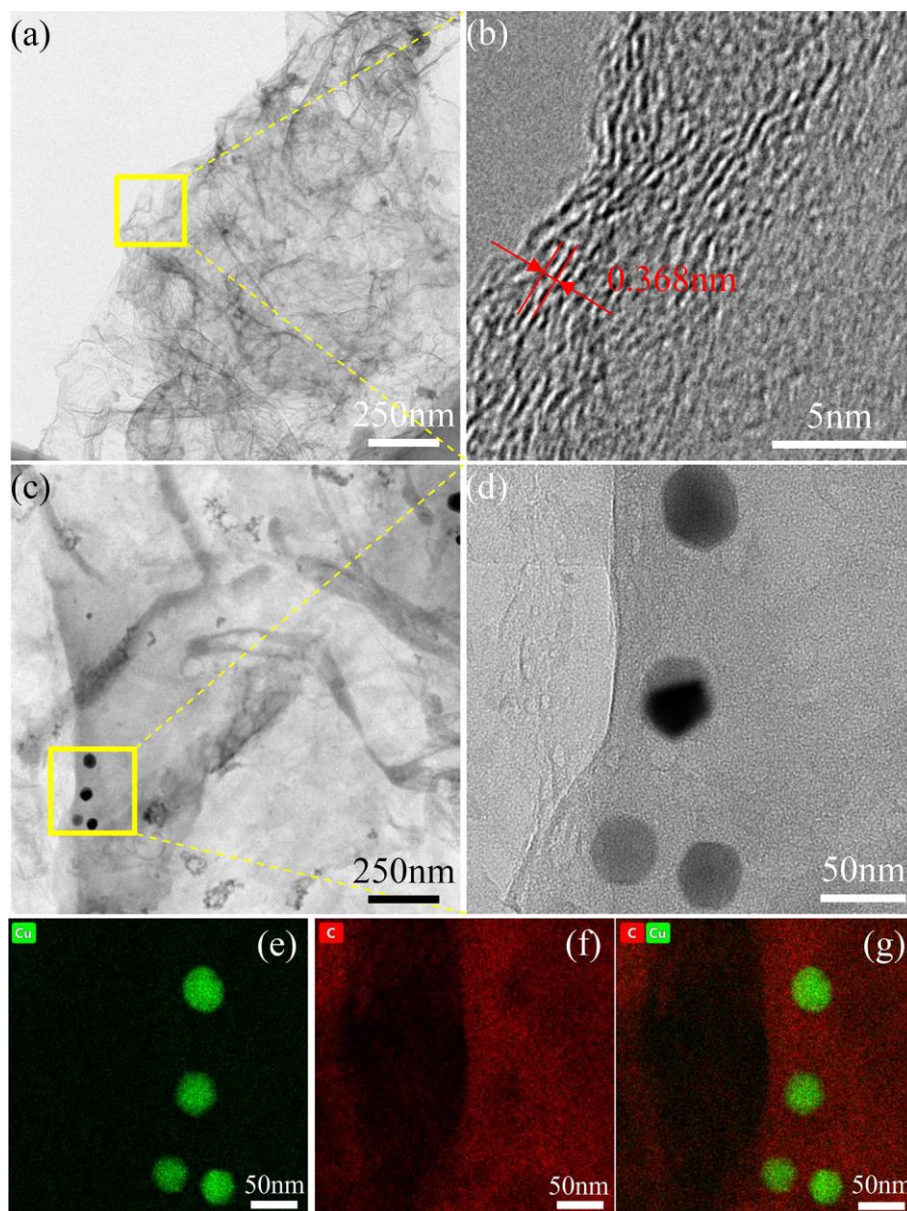


Fig. 7 TEM, HRTEM and EDS-Mapping images of 0.5Gr@Cu composite powder. (a) TEM, (b) HRTEM in the yellow box in (a), (c) TEM, (d) HRTEM in the yellow box in (c), (e~g) EDS-Mapping in the yellow box in (c)

Thermal analysis (Fig. 8) was carried out using protective atmosphere N_2 , and it can be seen that the thermal decomposition curve (TGA) of the flour showed two mass losses. The first mass loss in the temperature range of $38.9\sim 125.1\text{ }^\circ\text{C}$ corresponds to the removal of adsorbed water in the flour, and the second mass loss in the temperature range of $269\sim 508\text{ }^\circ\text{C}$ corresponds to the dehydration of the side

chain groups [38]. In addition, it can be seen from the DSC curve that only two mass losses are accompanied by exothermic peaks, and no other peaks appear in the subsequent heating, indicating that the carbon source tends to be stable under the catalysis of the copper-free substrate.

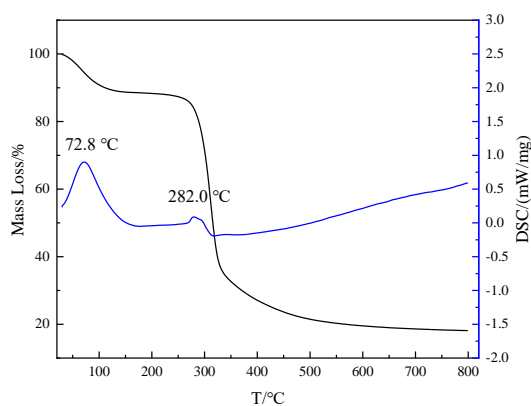


Fig. 8 TGA and DSC curves of wheat flour

The proposed mechanism of *in-situ* generation of Gr@Cu composite powder during the *in-situ* process is shown in Fig. 9. In the initial stage of heating (e.g., below 400°C), the Cu-O-Cu bonds in the original Cu₂O sheet react with the H-H bonds. At the following higher temperature stage, the chemical bonds obtain enough energy to re-arrange themselves. The copper ions are successfully reduced into copper, and the remained hydrogen ions and oxygen ions react and form water molecules, which are evaporated (Fig. 9(a)). With a further increase in temperature (800°C), the C-H and C=O bonds in the flour are reacted to form carbon atoms, which are adsorbed on the surface of copper particles. The remaining heteroatoms (e.g., O) are not adsorbed on the copper substrate due to the influence of the affinity with copper. In the subsequent process, the temperature is lowered in the H₂ atmosphere, and the carbon atoms which are originally adsorbed on the surface of the copper powder begin to be re-arranged.

In this process, the carbon on the surfaces of copper powders preferentially nucleate and eventually form graphene layers. The remaining heteroatoms are also recombined under the action of hydrogen ions and form the H₂O molecules, which are evaporated (Fig. 9(c)). In addition, although the flour contains a lot of oxygen atoms, no copper oxides are found at the bonding interface of graphene and copper. The reason may be attributed to that at the high temperature in the H₂ atmosphere, the affinity of carbon to the surface of the metal catalyst is higher than that of oxygen atoms. With the formation of graphene, the atomic rearrangement occurs, and the oxygen atoms are eliminated by the hydrogen [15] (Fig. 9 (c)).

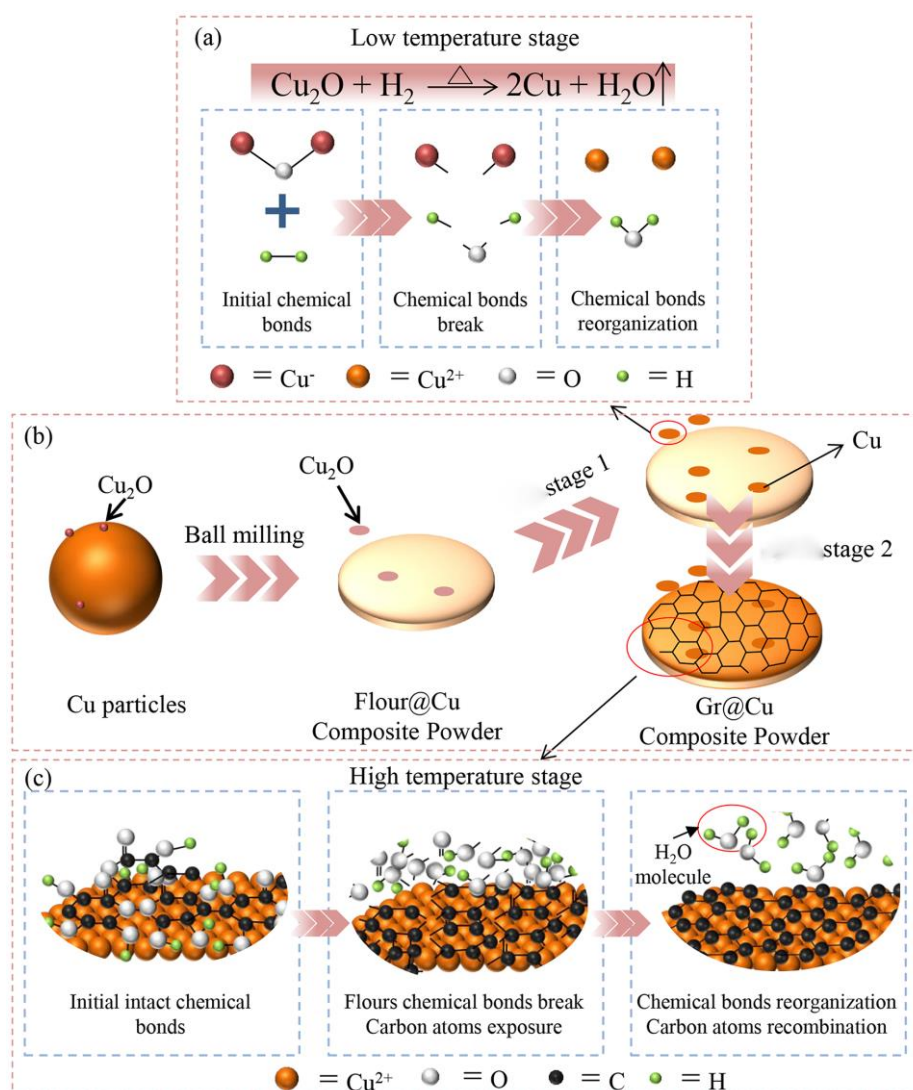


Fig. 9 Schematic diagram of the *in-situ* mechanism of in-situ Gr@Cu composite powder. (a) Cu₂O is reduced to Cu at the low-temperature stage, (b) Gr@Cu composite powder preparation process, (c) Gr formation at the high-temperature stage

Many studies reported that copper substrate has a certain catalytic effect for the *in-situ* grown graphene [11, 12, 15]. Therefore, in this paper, 0.5 g of flour was directly calcined and reduced by the same process technology, which was recorded as 0.5Gr. The catalytic effect of copper substrates was investigated using the Raman spectroscopy and XPS.

Fig. 10 shows the Raman spectra of 0.5Gr and unetched 0.5Gr@Cu. It can be seen from Fig. 10 that both these spectra have the characteristic peaks of carbon. Among them, the I_D/I_G value of 0.5Gr is 1.01, which is much larger than that of 0.5Gr@Cu composite powder. This indicates that without the catalysis of a copper substrate, the flour carbon source produces a lot of amorphous carbon, e.g., the defects are significantly increased. Under the catalysis of a copper substrate, the carbon source will be reduced into graphene, and its I_D/I_G value of 0.90 is consistent with that of the etched 0.5Gr@Cu (Fig. 6(c)).

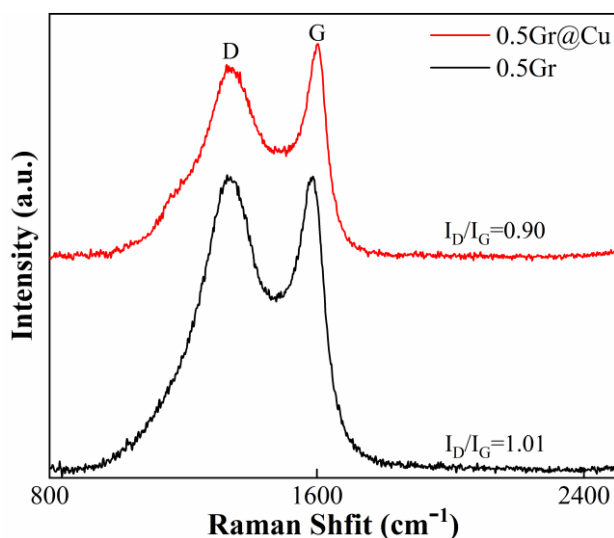


Fig. 10 Raman spectra of 0.5Gr and unetched 0.5Gr@Cu

Fig. 11 shows the XPS spectra of both the 0.5Gr and 0.5Gr@Cu, which can be used to extract the information of valence states and bond structures of graphene and copper. Fig. 11(a) shows the survey spectra of 0.5Gr and 0.5Gr@Cu. The existence of C and O elements can be seen from the XPS spectrum of 0.5Gr, and the characteristic binding energies of C 1s and O 1s are located at 284.8 eV and 531.8 eV, respectively. The survey spectrum of 0.5Gr@Cu shows that in addition to the presence of C and O elements, the Cu 2p characteristic peak of Cu element appears at 932.8 eV. Fig. 11(b) shows the high-resolution C 1s spectrum of 0.5Gr. It can be divided into four peaks at 284.4 eV, 284.8 eV, 286.1 eV and 288.9 eV, corresponding to sp^2 carbon (C=C), sp^3 carbon (C-C), C-O and C=O bonds, respectively. Fig. 11(c) shows the high-resolution C 1s spectrum of 0.5Gr@Cu, which can also be split into four peaks. Fig. 11(d) shows the high-resolution spectrum of copper element of 0.5Gr@Cu, in which the two peaks at 932.0 eV and 952.1 eV are assigned to Cu $2p^{3/2}$ and Cu $2p^{1/2}$ of Cu(0), respectively. Since the satellite peaks of copper oxide do not appear in the figure, this indicates that the original cuprous oxide has been reduced when graphene is *in-situ* formed, and the

heteroatoms in the carbon source will not oxidize the copper substrate [11]. These results are the same with those of XRD, and prove the graphene formation mechanism (e.g., Fig. 4 and Fig. 9, respectively). The ratios of different carbon bonds in 0.5Gr and 0.5Gr@Cu are shown in Fig. 11(e). It is obvious that the proportion of sp^2 carbon (C=C) increases and the proportion of sp^3 carbon (C-C) decreases when the copper substrate is present. The results are consistent with the Raman analysis results, which show that the copper matrix can reduce the defects of graphene (Fig. 10). Both the Raman and XPS results confirm that the copper substrate has a good ability to catalyze the carbon source to form graphene.

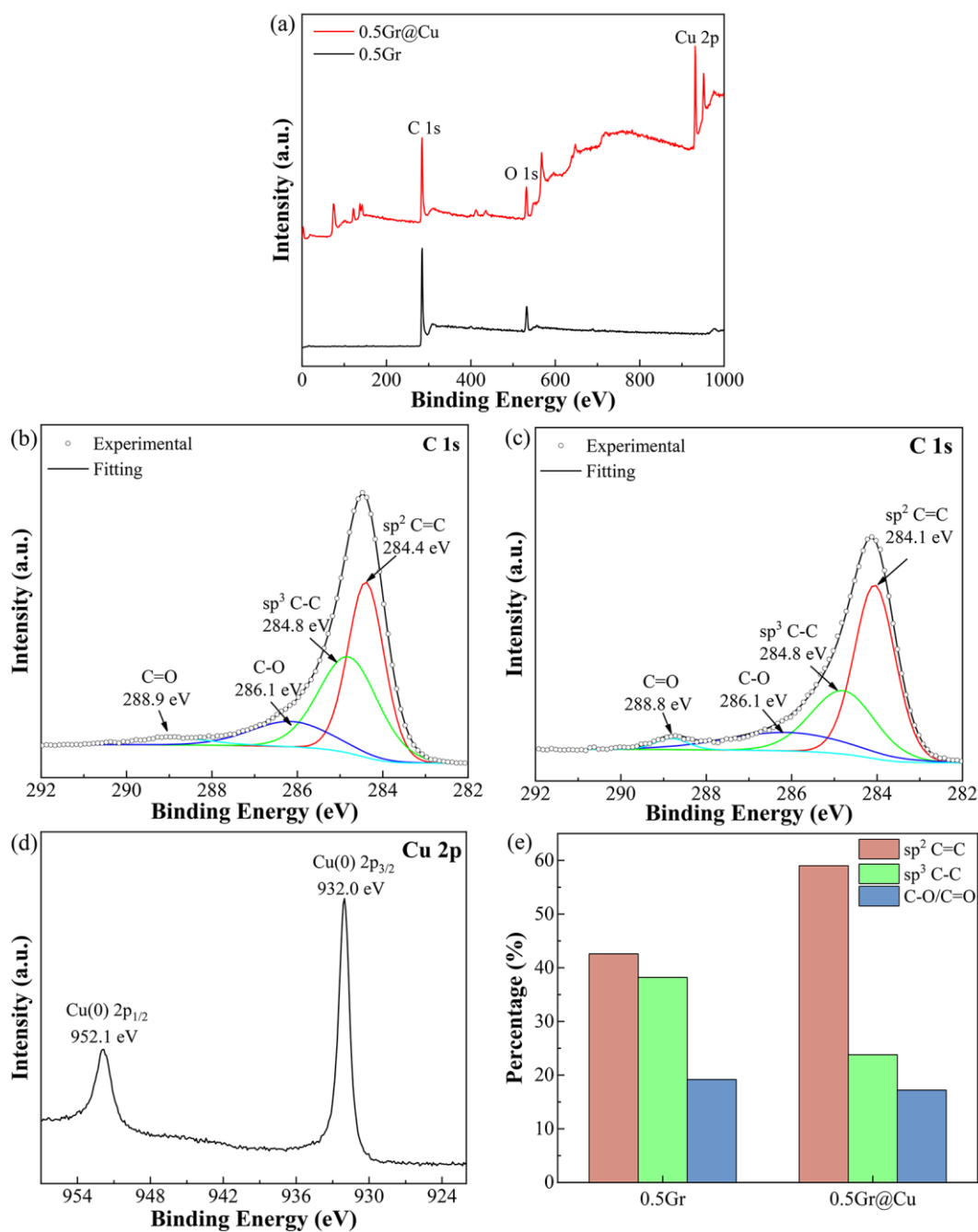


Fig. 11 XPS spectra of 0.5Gr and 0.5Gr@Cu. (a) Full spectrum, (b) C 1s spectrum of 0.5Gr, (c) C 1s spectrum of 0.5Gr@Cu, (d) Cu 2p spectrum of 0.5Gr@Cu, (e) Ratios of different carbon bonds in 0.5Gr and 0.5Gr@Cu

We further obtained the HRTEM image of 0.5Gr@Cu composite powder, along with its Fast Fourier Transform (FFT) and Inverse Fast Fourier Transform (IFFT) images at the interfacial region (Fig. 12). The aim is to study the nature of crystal

bonding between *in-situ* generated Gr and Cu substrate and the degree of lattice mismatch. Fig. 12(b) shows the three-layer structures. The lattice fringe spacing of the innermost layer is ~ 0.212 nm, which is similar to the $\text{Cu}_{(111)}$ crystal plane spacing of 0.208 nm, indicating that this should be from the copper powder. The middle layer is a 4-6 nm black composite interface layer, and the lattice fringes have shown certain curvatures can be observed. The spacing is 0.368 nm, which is near to the $\text{Gr}_{(002)}$ crystal plane spacing of 0.34 nm. The bright and white area in the outermost layer is the pure graphene layer. Figs. 12(c) and 10(c1) are the FFT and IFFT diagrams in the yellow box of Fig. 12(b), respectively, and the detailed analysis shows that the crystal orientation relationship between Gr and Cu is following $\text{Cu}_{\{111\}}//\text{Gr}_{\{002\}}$. This crystal orientation is not perfectly parallel but has an orientation difference of 29.4° (Fig. 12(c1)). The similar crystalline orientation relationship between graphene and copper has been reported in literature [14, 17]. The presence of poor orientation mismatch causes the formation of circular lattice fringes of graphene to appear in the HRTEM image (Fig. 12(b)). This is because the Gr usually maintains a 29° orientation difference with the $\{111\}$ crystal plane group of copper.

On the other hand, we noticed that the lattice fringe spacings of both Gr and Cu are larger than their normal values. This may be due to the thermal stress generated after the *in-situ* process, which causes the generation of tensile stress and formation of more dislocation or defects at their interfaces. To verify this, we did the FFT of the $\text{Gr}_{(002)}$ crystal plane and $\text{Cu}_{(111)}$ crystal plane generated by 0.5 g of flour and then performed IFFT on them. The results show that the lattice fringes of Gr not only are

bent, but also show a large number of dislocations in the lattice fringes of Gr, which are represented by the symbol “T” in Fig. 12(d). Whereas the lattice fringes of Cu only show bending phenomenon (Fig. 12(d₁)). The bending of lattice fringes and the generation of dislocations are strong evidences of the increase in the spacing of lattice fringes. One of the reasons for this phenomenon is the large difference in the thermal expansion between graphene and copper, which generates a large thermal stress and increases the interplanar spacing [17]. The interfaces do not show intermediate phase and cracks/pores.

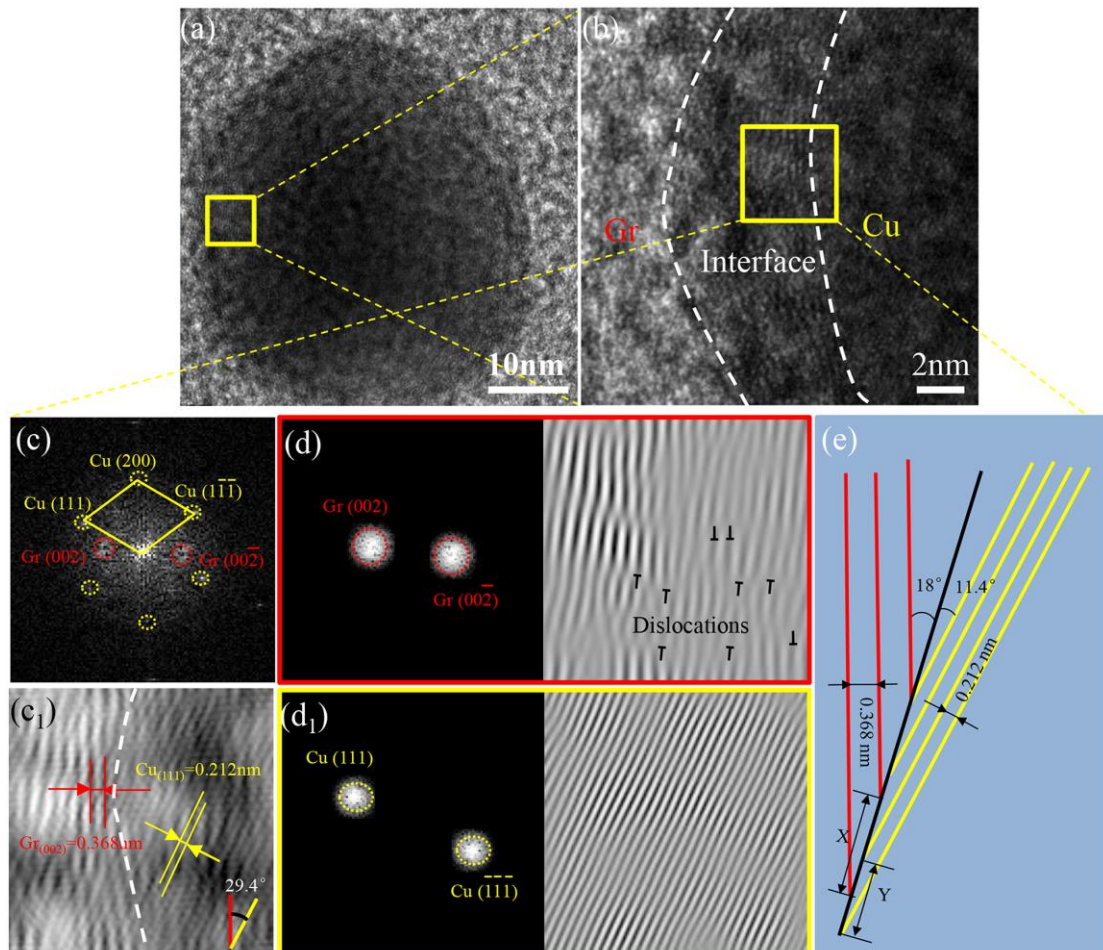


Fig. 12 HRTEM, FFT and IFFT images of 0.5Gr@Cu composite powder. (a) Low magnification HRTEM, (b) High magnification HRTEM, (c) FFT in the yellow box in

(b), (c1) IFFT in the yellow box in (b), (d) IFFT of Gr₍₀₀₂₎, (d1) IFFT of Cu₍₁₁₁₎, (e) the schematic diagram of the interface of (c1). We selected Gr₍₀₀₂₎ (red line) and Cu₍₁₁₁₎ (yellow line), and then drew multiple parallel lines, and then obtained the interface angle between Gr and Cu

A good crystallographic matching helps to form a low-energy interface when the two interfaces of different phases are bonded, and this will have enhancing effects on the stability and bonding strength of the interfacial structures [39]. The interface mismatch (δ) is an important parameter to show the matching relationship between the two phases. We calculated the mismatch degree of 0.5Gr@Cu composite powder using the calculation formula (1)[40].

$$\delta = \frac{d_2 - d_1}{d_1} \quad (1)$$

where d_1 and d_2 are the interplanar spacing of Cu₍₁₁₁₎ and Gr₍₀₀₂₎, respectively. However, the interface between graphene and copper has a certain bending angle (Fig. 12(c1)). For this type of angled interface, the length of X and Y can be obtained according to Fig. 12(e), and then the degree of interface mismatch can be calculated using formula (2) [40]. According to the schematic diagram of the interface shown in Fig. 12(e), the angle between Gr and the interface is $\sim 18^\circ$, and the angle between Cu and the interface is $\sim 11.4^\circ$. The Gr₍₀₀₂₎ crystal plane spacing is 0.368 nm, and the Cu₍₁₁₁₎ crystal plane is 0.212 nm. Therefore, we obtained X=1.191 nm and Y=1.073 nm according to the trigonometric function, and a δ value of 11% can be obtained. As we know that when $5\% < \delta < 25\%$, the interface is a semi-coherent one [41]. Therefore, the Gr₍₀₀₂₎ and Cu₍₁₁₁₎ have a semi-coherent interface, e.g., $\delta = \frac{X-Y}{Y} = 11\% < 25\%$. This kind

of semi-coherent interface often generates dislocations in order to reduce the large elastic strain energy at the interface, which is another key factor to cause the generation of dislocations at the interfaces between Gr and Cu [42].

Through this semi-coherent relationship, a new interpretation for the formation of interface dislocations can be made. Li [43] et al. and Zhang [44] et al. observed dislocations at the composite interface of graphene and copper, however, they assumed that this was caused by the difference in the coefficient of thermal expansion between two phases. Our results indicate that this should be a combined effect from thermal expansion coefficient mismatch and a special semi-coherent relationship between these two phases. In addition, the semi-coherent interface does not have a strong interfacial strength as that in the coherent interface. For the graphene reinforced copper matrix composites, graphene is often observed to be pulled out from the fracture surfaces [24, 34]. Therefore, the enhancement effect of graphene on the copper matrix is not as significant as expected from the theoretical model.

As shown in Fig. 13, many researchers used intermediate particles to improve the interfacial bonding between graphene and copper. Their results show that the mechanical properties of the composite materials obtained through applying these intermediate particles have been improved but the effects are quite different [45-50]. These intermediate particles have been verified to improve the wettability and interfacial bonding of graphene and copper.

Our study in this paper shows the semi-coherent interface bonding relationship between graphene and copper. Based on these results, we can assume that the

intermediate phases are formed along with copper or graphene, and the bonding between copper and graphene has formed a coherent interface. Due to this change of interfacial bonding characteristics at the interfaces caused by these intermediate particles, the enhancement effects of strength can be significantly improved. In addition, compared to the non-coherent interface, the formed semi-coherent interface will increase the strain hardening effect due to the presence of dislocations, which indicates that our *in-situ* strategy successfully achieves a strong interfacial interaction between graphene and copper.

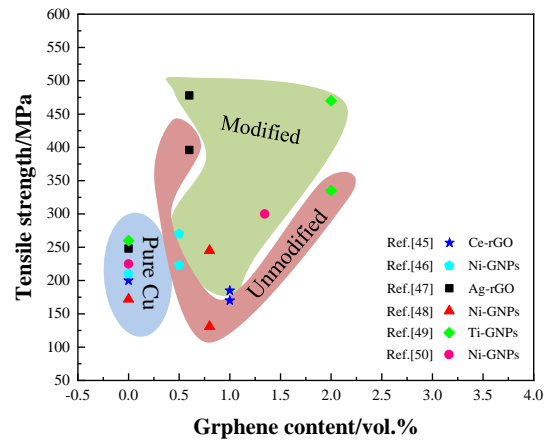


Fig. 13 Comparison of tensile strength of metal particle modified and unmodified graphene reinforced copper matrix composites

4. Conclusion

In this work, we proposed a new methodology to use wheat flour as a solid carbon source to *in-situ* generate graphene on the surfaces of Cu powders. A ball milling process was used to uniformly mix different contents of flour and copper powder, and then an *in-situ* generation process was used to obtain high-quality Gr@Cu composite powder. Following conclusions were obtained from this study.

(1) When the carbon source content was reduced from 1.0 g to 0.5 g, the *in-situ* generated layered material was changed from a thick GLNP to a thin Gr layer.

(2) *In-situ* generation mechanism of graphene on the surface of copper powder can be explained from the changes in two stages. In the low temperature stage (up to 400 °C), cuprous oxide was reduced by H₂; whereas in the high temperature stage (269-800 °C), the carbon sources were decomposed and recombined to form a layer of graphene.

(3) The interfaces between the graphene and the copper matrix were well bonded, with a lattice orientation relationship of Cu(111)//Gr(002), and their interface was a semi-coherent one.

Acknowledgment

The authors would like to acknowledge the financial supports from Shaanxi Coal Industry Group United Fund of China (No.2019JLM-2), Xi'an Science research project of China (No.2020KJRC0089) and Electrical Materials and Infiltration Key Laboratory of Shaanxi Province Projects (No.17JS080), and International Exchange Grant (IEC/NSFC/201078) through Royal Society and National Science Foundation of China (NSFC).

Conflict of Interest

The authors declare no conflict of interest.

References

- [1] D. Ponnamma, Y. Yin, N. Salim, J. Parameswaranpillai, S. Thomas, N. Hameed, Recent progress and multifunctional applications of 3D printed graphene nanocomposites, *Composites Part B: Engineering* 204 (2021) 108493.
- [2] Z. Zhao, P. Bai, W. Du, B. Liu, D. Pan, R. Das, C. Liu, Z. Guo, An overview of graphene and its derivatives reinforced metal matrix composites: Preparation, properties and applications, *Carbon* 170 (2020) 302-326.
- [3] I. Baldea, D. Olteanu, G.A. Filip, F. Pogacean, M. Coros, M. Suci, S.C. Tripon, M. Cenariu, L. Magerusan, R.-I. Stefan-van Staden, S. Pruneanu, Cytotoxicity mechanisms of nitrogen-doped graphene obtained by electrochemical exfoliation of graphite rods, on human endothelial and colon cancer cells, *Carbon* 158 (2020) 267-281.
- [4] K.S. Novoselov, A.K. Geim, S.V. Morozov, D.S. Jiang, Y. Zhang, S.V. Dubonos, I.V. Grigorieva, A.A. Firsov, Electric Field Effect in Atomically Thin Carbon Films, *Science* 306(5696) (2004) 666-669.
- [5] S. Stankovich, D.A. Dikin, R.D. Piner, K.A. Kohlhaas, A. Kleinhammes, Y. Jia, Y. Wu, S.T. Nguyen, R.S. Ruoff, Synthesis of graphene-based nanosheets via chemical reduction of exfoliated graphite oxide, *Carbon* 45(7) (2007) 1558-1565.
- [6] F. Chen, Q.S. Mei, J.Y. Li, C.L. Li, L. Wan, G.D. Zhang, X.M. Mei, Z.H. Chen, T. Xu, Y.C. Wang, Fabrication of graphene/copper nanocomposites via in-situ delamination of graphite in copper by accumulative roll-compositing, *Composites Part B: Engineering* 216 (2021) 108850.
- [7] B. Claire, Electronic confinement and coherence in patterned epitaxial graphene, *Science* 5777(312) (2006) 1191-1196.
- [8] P.R. Somani, S.P. Somani, M. Umeno, Planer nano-graphenes from camphor by CVD, *Chemical Physics Letters* 430(1) (2006) 56-59.
- [9] A. Srivastava, C. Galande, L. Ci, L. Song, C. Rai, D. Jariwala, K.F. Kelly, P.M. Ajayan, Novel Liquid Precursor-Based Facile Synthesis of Large-Area Continuous, Single, and Few-Layer Graphene Films, *Chemistry of Materials* 22(11) (2010) 3457-3461.
- [10] Y. Chen, X. Zhang, E. Liu, C. He, C. Shi, J. Li, P. Nash, N. Zhao, Fabrication of in-situ grown graphene reinforced Cu matrix composites, *Scientific Reports* 6(1) (2016) 19363.
- [11] X. Zhang, C. Shi, E. Liu, F. He, L. Ma, Q. Li, J. Li, W. Bacs, N. Zhao, C. He, Achieving high strength and high ductility in metal matrix composites reinforced with a discontinuous three-dimensional graphene-like network, *Nanoscale* 9(33) (2017) 11929-11938.
- [12] X. Li, W. Cai, J. An, S. Kim, J. Nah, D. Yang, R. Piner, A. Velamakanni, I. Jung, E. Tutuc, S.K. Banerjee, L. Colombo, R.S. Ruoff, Large-Area Synthesis of High-Quality and Uniform Graphene Films on Copper Foils, *Science* 324(5932) (2009) 1312-1314.
- [13] Z. Gao, T. Zuo, M. Wang, L. Zhang, B. Da, Y. Ru, J. Xue, Y. Wu, L. Han, L. Xiao, In-situ graphene enhanced copper wire: A novel electrical material with

simultaneously high electrical conductivity and high strength, *Carbon* 186 (2022) 303-312.

[14] X. Zhang, C. Shi, E. Liu, N. Zhao, C. He, Effect of Interface Structure on the Mechanical Properties of Graphene Nanosheets Reinforced Copper Matrix Composites, *ACS Applied Materials & Interfaces* 10(43) (2018) 37586-37601.

[15] Z. Sun, Z. Yan, J. Yao, E. Beitler, Y. Zhu, J.M. Tour, Growth of graphene from solid carbon sources, *Nature* 468(7323) (2010) 549-552.

[16] S. Wang, X. Huang, Y. He, H. Huang, Y. Wu, L. Hou, X. Liu, T. Yang, J. Zou, B. Huang, Synthesis, growth mechanism and thermal stability of copper nanoparticles encapsulated by multi-layer graphene, *Carbon* 50(6) (2012) 2119-2125.

[17] C. Sun, X. Zhang, N. Zhao, C. He, Influence of spark plasma sintering temperature on the microstructure and strengthening mechanisms of discontinuous three-dimensional graphene-like network reinforced Cu matrix composites, *Materials Science and Engineering: A* 756 (2019) 82-91.

[18] S. Lee, J. Hong, J.H. Koo, H. Lee, S. Lee, T. Choi, H. Jung, B. Koo, J. Park, H. Kim, Y.-W. Kim, T. Lee, Synthesis of Few-Layered Graphene Nanoballs with Copper Cores Using Solid Carbon Source, *ACS Applied Materials & Interfaces* 5(7) (2013) 2432-2437.

[19] K. Chu, F. Wang, Y.-b. Li, X.-h. Wang, D.-j. Huang, Z.-r. Geng, Interface and mechanical/thermal properties of graphene/copper composite with Mo₂C nanoparticles grown on graphene, *Composites Part A: Applied Science and Manufacturing* 109 (2018) 267-279.

[20] T. Zuo, M. Wang, J. Xue, Y. Ru, L. Zhang, B. Da, Y. Wu, Z. Xu, Z. Gao, P.K. Liaw, L. Han, L. Xiao, Superior electrical conductivity-strength combination of an in-situ fabricated La₂O₃-doped copper/graphene composite conductor, *Carbon* 197 (2022) 455-465.

[21] T. Yang, W. Chen, H. Zhang, L. Ma, Y.-Q. Fu, In-situ generated graphene from wheat flour for enhancing mechanical and electrical properties of copper matrix composites, *Materials Science and Engineering: A* 835 (2022) 142662.

[22] G. Lin, Y. Peng, Z. Dong, D.-B. Xiong, Tribology behavior of high-content graphene/nanograined Cu bulk composites from core/shell nanoparticles, *Composites Communications* 25 (2021) 100777.

[23] S. Shu, Q. Yuan, W. Dai, M. Wu, D. Dai, K. Yang, B. Wang, C.-T. Lin, T. Wuebben, J. Degenhardt, C. Regula, R. Wilken, N. Jiang, J. Ihde, In-situ synthesis of graphene-like carbon encapsulated copper particles for reinforcing copper matrix composites, *Materials & Design* 203 (2021) 109586.

[24] S. Guo, X. Zhang, C. Shi, E. Liu, C. He, F. He, N. Zhao, In situ synthesis of high content graphene nanoplatelets reinforced Cu matrix composites with enhanced thermal conductivity and tensile strength, *Powder Technology* 362 (2020) 126-134.

[25] S. Wang, S. Han, G. Xin, J. Lin, R. Wei, J. Lian, K. Sun, X. Zu, Q. Yu, High-quality graphene directly grown on Cu nanoparticles for Cu-graphene nanocomposites, *Materials & Design* 139 (2018) 181-187.

[26] B. Deng, J. Wu, S. Zhang, Y. Qi, L. Zheng, H. Yang, J. Tang, L. Tong, J. Zhang, Z. Liu, H. Peng, Anisotropic Strain Relaxation of Graphene by Corrugation on Copper

- Crystal Surfaces, *Small* 14(22) (2018) 1800725.
- [27] T. Cheng, L. Sun, Z. Liu, F. Ding, Z. Liu, Roles of Transition Metal Substrates in Graphene Chemical Vapor Deposition Growth, *Acta Physico-Chimica Sinica* (2021) 1-16.
- [28] B.W. Li, D. Luo, L. Zhu, X. Zhang, S. Jin, M. Huang, F. Ding, R.S. Ruoff, Orientation - Dependent Strain Relaxation and Chemical Functionalization of Graphene on a Cu(111) Foil, *Advanced Materials* 30(10) (2018) 201706504.
- [29] M.S. Dresselhaus, A. Jorio, M. Hofmann, G. Dresselhaus, R. Saito, Perspectives on Carbon Nanotubes and Graphene Raman Spectroscopy, *Nano Letters* 10(3) (2010) 751-758.
- [30] X. Liu, J. Li, E. Liu, Q. Li, C. He, C. Shi, N. Zhao, Effectively reinforced load transfer and fracture elongation by forming Al₄C₃ for in-situ synthesizing carbon nanotube reinforced Al matrix composites, *Materials Science and Engineering: A* 718 (2018) 182-189.
- [31] R. sayyad, M. Ghambari, T. Ebadzadeh, A.H. Pakseresht, E. Ghasali, Preparation of Ag/reduced graphene oxide reinforced copper matrix composites through spark plasma sintering: An investigation of microstructure and mechanical properties, *Ceramics International* 46(9) (2020) 13569-13579.
- [32] B. Lee, M.Y. Koo, S.H. Jin, K.T. Kim, S.H. Hong, Simultaneous strengthening and toughening of reduced graphene oxide/alumina composites fabricated by molecular-level mixing process, *Carbon* 78 (2014) 212-219.
- [33] C. Zhao, J. Wang, Fabrication and tensile properties of graphene/copper composites prepared by electroless plating for structural applications, *Physica Status Solidi A-Applications and Materials Science* 211(12) (2014) 2878-2885.
- [34] K. Zhang, G. Shao, X. Chen, W. Li, F. Ma, P. Liu, Study of mechanical properties of graphene nanoplates reinforced copper matrix composites prepared through electrostatic self-assembly and electroless copper plating, *Materials Letters* 252 (2019) 338-341.
- [35] O. Frank, G. Tsoukleri, J. Parthenios, K. Papagelis, I. Riaz, R. Jalil, K.S. Novoselov, C. Galiotis, Compression Behavior of Single-layer Graphene, *ACS Nano* 4(6) (2010) 3131-3138.
- [36] X. Zhang, C. Shi, E. Liu, J. Li, N. Zhao, C. He, Nitrogen-doped graphene network supported copper nanoparticles encapsulated with graphene shells for surface-enhanced Raman scattering, *Nanoscale* 7(40) (2015) 17079-17087.
- [37] X. Zhang, Y. Xu, M. Wang, E.Z. Liu, C. He, A powder-metallurgy-based strategy toward three-dimensional graphene-like network for reinforcing copper matrix composites, *Nature Communications* 11(1) (2020) 2775.
- [38] P. Aggarwal, D. Dollimore, A thermal analysis investigation of partially hydrolyzed starch, *Thermochimica Acta* 319(1) (1998) 17-25.
- [39] H.-Y. Yang, Z.-J. Cai, Q. Zhang, Y. Shao, B.-X. Dong, Q.-Q. Xuan, F. Qiu, Comparison of the effects of Mg and Zn on the interface mismatch and compression properties of 50 vol% TiB₂/Al composites, *Ceramics International* (2021).
- [40] S.Y. Qian, Z.H. Xu, H.N. Xie, C.S. Shi, N.Q. Zhao, C.N. He, E.Z. Liu, Effect of rare metal element interfacial modulation in graphene/Cu composite with high

strength, high ductility and good electrical conductivity, *Applied Surface Science* 533 (2020) 147489.

[41] W. Peng, K. Sun, Effects of Cu/graphene interface on the mechanical properties of multilayer Cu/graphene composites, *Mechanics of Materials* 141 (2020) 103270.

[42] M. Cao, D.-B. Xiong, Z. Tan, G. Ji, B. Amin-Ahmadi, Q. Guo, G. Fan, C. Guo, Z. Li, D. Zhang, Aligning graphene in bulk copper: Nacre-inspired nanolaminated architecture coupled with in-situ processing for enhanced mechanical properties and high electrical conductivity, *Carbon* 117 (2017) 65-74.

[43] X. Li, S. Yan, X. Chen, Q. Hong, N. Wang, Microstructure and mechanical properties of graphene-reinforced copper matrix composites prepared by in-situ CVD, ball-milling, and spark plasma sintering, *Journal of Alloys and Compounds* 834 (2020) 155182.

[44] D. Zhang, Z. Zhan, Strengthening effect of graphene derivatives in copper matrix composites, *Journal of Alloys and Compounds* 654 (2016) 226-233.

[45] M. Li, H. Che, X. Liu, S. Liang, H. Xie, Highly enhanced mechanical properties in Cu matrix composites reinforced with graphene decorated metallic nanoparticles, *Journal of Materials Science* 49(10) (2014) 3725-3731.

[46] H. Luo, Y. Sui, J. Qi, Q. Meng, F. Wei, Y. He, Mechanical enhancement of copper matrix composites with homogeneously dispersed graphene modified by silver nanoparticles, *Journal of Alloys and Compounds* 729 (2017) 293-302.

[47] X. Si, M. Li, F. Chen, P. Eklund, J. Xue, F. Huang, S. Du, Q. Huang, Effect of carbide interlayers on the microstructure and properties of graphene-nanoplatelet-reinforced copper matrix composites, *Materials Science and Engineering: A* 708 (2017) 311-318.

[48] T. Yang, W. Chen, F. Yan, H. Lv, Y.Q. Fu, Effect of reduced graphene oxides decorated by Ag and Ce on mechanical properties and electrical conductivity of copper matrix composites, *Vacuum* 183 (2021) 109861.

[49] D. Zhang, Z. Zhan, Preparation of graphene nanoplatelets-copper composites by a modified semi-powder method and their mechanical properties, *Journal of Alloys and Compounds* 658 (2016) 663-671.

[50] T. Han, J. Li, N. Zhao, C. He, Fabrication of Graphene Nanoplates Modified with Nickel Nanoparticles for Reinforcing Copper Matrix Composites, *Acta Metallurgica Sinica (English Letters)* 33(5) (2020) 643-648.